Chern insulator phases and spontaneous spin and valley order in a moiré lattice model for magic-angle twisted bilayer graphene

Clara N. Breiø and Brian M. Andersen
Niels Bohr Institute, University of Copenhagen, 2100 Copenhagen, Denmark

(Received 30 October 2022; accepted 27 March 2023; published 7 April 2023)

At a certain "magic" relative twist angle of two graphene sheets it remains a challenge to obtain a detailed description of the proliferation of correlated topological electronic phases and their filling dependence. We perform a self-consistent real-space Hartree-Fock study of an effective moiré lattice model to map out the preferred ordered phases as a function of Coulomb interaction strength and moiré flat-band filling factor. It is found that a quantum valley Hall phase, previously discovered at charge neutrality, is present at all integer fillings for sufficiently large interactions. However, except for charge neutrality, additional spontaneous spin/valley polarization is present in the ground state at nonzero integer fillings, leading to Chern insulator phases and anomalous quantum Hall effects at odd filling factors, thus constituting an example of interaction-driven nontrivial topology. At weaker interactions, all nonzero integer fillings feature metallic inhomogeneous spin/valley ordered phases which may also break additional point group symmetries of the system. We discuss these findings in the light of previous theoretical studies on and recent experimental developments related to magic-angle twisted bilayer graphene.

DOI: 10.1103/PhysRevB.107.165114

I. INTRODUCTION

Magic-angle twisted bilayer graphene (MATBG) provides a tunable platform for studying the properties of strongly correlated electrons on moiré superlattices [1–4]. The moiré lattice is generated by the relative twist, which may, at certain angles, lead to very narrow low-energy minibands hosting electrons with large interactions relative to their respective kinetic energy [5–7]. At the magic angle of $\theta \simeq 1.1^\circ$ the flat bands are well separated from the dispersive bands at higher energies. An incipient Berry curvature of the moiré flat bands additionally imprints the correlated electronic states with nontrivial topology. The resulting emergent electronic behavior includes both unusual normal state properties and the formation of different electronic phases exhibiting magnetic and superconducting signatures at low temperatures [3,4]. Thus, MATBG is interesting in its own right and may also help shed light on the more general outstanding questions pertaining to strange-metal behavior and the origin of unconventional superconductivity [1,2]. Therefore, it is important to understand this system and elucidate the nature of the emergent electronic phases appearing in MATBG moiré superlattices.

Experimentally, a series of mainly transport and scanning tunneling spectroscopy (STS) measurements on MATBG has investigated its phase diagram as a function of temperature and electronic density, reporting correlated insulating states at integer filling factors separated by superconducting domes at the lowest temperatures [1,2,8–15]. At some filling factors of the moiré flat bands, there is evidence of magnetism and quantum anomalous Hall response [8,13,16–19]. Other correlated states under consideration include Chern insulators and nematic phases also at integer moiré band filling [20–23] and translation symmetry-breaking spin or charge density wave order at certain half-integer fillings [24]. Local electronic compressibility and STS measurements recently revealed a sequence of distinct phase transitions near the integer fillings of the moiré unit cell, establishing a cascade of transitions associated with split-off bands of particular spin or valley character [25–27]. The detailed properties of the phase diagram appear to depend rather sensitively on the twist angle, substrate potential, or degree of alignment of one of the graphene sheets with the hexagonal boron nitride encapsulation layers, which breaks an inherent C_2 symmetry of the graphene bilayer itself [8,9,17,18]. The twist-generated correlated phases have also been explored in other graphene-based systems, including twisted trilayers and twisted double bilayer graphene. Such stacked graphene sheets also feature rich phase diagrams with superconductivity and tunable insulator states, sensitive to both twist angle and electric displacement field [28–32].

Theoretically, the existence of insulating states in MATBG has been addressed with a large variety of techniques and approximations [33–70]. The search for a detailed quantitative theoretical description of the origin and interplay of different flavor-ordered phases and their dependence on, e.g., filling and twist angle is still ongoing. These efforts are important not only from the perspective of understanding transport and tunneling measurements but potentially also for identifying the "normal state" from which superconductivity emerges at lower temperatures. From the perspective of Hartree-Fock (HF) approximated interactions, such an approach can lead to insulating behavior from induced order, causing a spectral gap, typically arising from one or more spontaneously broken symmetries of the original Hamiltonian. Application of HF theory to handle electronic interactions has been widely applied to MATBG in order to describe the correlated

insulator phases [48,54,57,58,60–62,65,67,69]. Such studies have proposed, depending on the band filling factor, a rather large variety of spontaneously symmetry broken candidate phases relevant for MATBG. These include spin and valley ferromagnetic phases, intervalley coherent insulators, valence bond solids, nematic semimetals, quantum valley Hall and quantum spin Hall insulators, incommensurate Kekulé spiral order, and various other forms of inhomogeneous density wave order [33–69].

Most theoretical works depart from the Bistritzer-MacDonald model with extended continuum wave functions and Coulomb interactions projected into the continuum states, including a number of the remote bands. A complementary Wannier description to study the correlated phases of MATBG was suggested by Kang and Vafek in which the Coulomb interaction is projected onto the localized Wannier states of the four spin-degenerate moiré flat bands [38]. Due to Wannier obstruction, symmetry requirements within this framework lead to crucial nonlocal assisted-hopping-like interaction terms in real space [38]. A previous work studied the effect of these assisted-hopping interactions on the ground state of MATBG at charge neutrality via HF mean-field studies and quantum Monte Carlo (QMC) simulations [65]. It was found that the normal state Dirac semimetal phase was unstable and insulating already at weak coupling, which was a consequence of an induced quantum valley Hall (QVH) phase [65]. Upon variation of the relative strength of the assisted-hopping interactions and overall interaction strength, several other insulating phases were found to emerge. These include (1) on-site intervalley coherence (IVC) order, which breaks the spin-valley SU(4) symmetry of the interacting part of the model, and (2) an insulating columnar valence bond solid state. A main result of Ref. [65] was the importance of the assisted-hopping term in stabilizing the QVH and IVC states. It was concluded, therefore, that an experimental observation of these quantum states at charge neutrality would provide evidence of the importance of nonlocal topologically driven interactions in MATBG.

Here, we extend the HF studies of Ref. [65] to address other filling factors of the moiré flat bands. We perform an unrestricted mean-field real-space study which allows for both homogeneous and inhomogeneous solutions. In the former case, we benchmark the results against a momentum-space formalism, which additionally allows for determination of the interaction-renormalized band structure. Our theoretical study focuses on the case of zero external magnetic field. At charge neutrality we find that interactions induce a gapped homogeneous QVH phase, in agreement with earlier studies using the same model [65]. At other integer fillings, the QVH phases coexists with spin/valley-flavor symmetry-broken order, consisting of spin/valley polarized phases for interaction strengths larger than approximately the bandwidth. We analyze the topological properties of the resulting gapped phases where the spontaneous order has lifted the degeneracy of the flavor symmetries of the bare band. For weaker interaction strengths at nonzero integer filling factors or at certain half-integer fillings, the model prefers metallic inhomogeneous spin- and valley-ordered phases. We analyze these results in light of recent experimental developments related to MATBG.

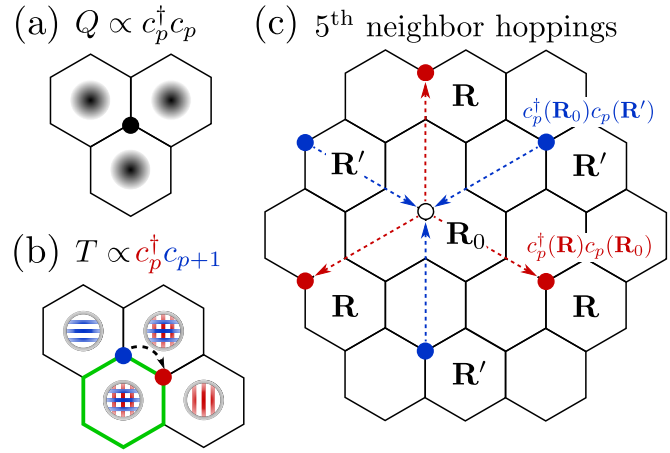

FIG. 1. (a) Illustration of the cluster charge term $Q(\mathbf{R})$ entering Eq. (1). Shaded gray areas are the density distribution of a Wannier orbital at the honeycomb site marked by a black dot. (b) Schematic of the assisted-hopping term $T(\mathbf{R})$. Blue horizontal (red vertical) lines show the density distribution of a Wannier orbital centered at the blue (red) honeycomb site. The overlap within the hexagon highlighted in green is finite and non-negligible. (c) Fifth NN hoppings in H_0. Hoppings marked in blue are the terms in the $\mathbf{R}'$ summation for $\mathbf{R} = \mathbf{R}_0$, and hoppings marked in red are included when the $\mathbf{R}$ summation reaches hexagons marked by $\mathbf{R}$ and $\mathbf{R}' = \mathbf{R}_0$.

II. MODEL AND METHOD

Constructing an interacting lattice Hamiltonian modeling MATBG is complicated due to the fragile topology of the narrow bands preventing a faithful representation in terms of standard localized Wannier orbitals, a property known as Wannier obstruction [71,72]. To overcome this obstruction one must either add (trivial) remote bands by including additional orbitals or implement some of the required symmetries nonlocally by including longer-range interactions. The model presented by Kang and Vafek [38] takes the latter approach and implements the $C_2\mathcal{T}$ symmetry nonlocally, where C_2 refers to a twofold rotation with respect to the z axis and $\mathcal{T}$ denotes time reversal. This procedure allows for a projection of the screened Coulomb potential to the appropriate low-energy Wannier orbitals residing on a bipartite honeycomb lattice [38,73]. The projection was performed in Ref. [38] and led to the following interaction term:

$$H_{\text{int}} = \frac{U}{2}\sum_{\mathbf{R}}[Q(\mathbf{R}) + T(\mathbf{R})]^2, \tag{1}$$

where

$$Q(\mathbf{R}) = \frac{1}{3}\sum_{p=0}^{5}\sum_{\tau,\sigma} c^\dagger_{p\tau\sigma}(\mathbf{R})c_{p\tau\sigma}(\mathbf{R}) \tag{2}$$

and

$$T(\mathbf{R}) = \alpha\sum_{p=0}^{5}\sum_{\tau,\sigma}(-1)^p[c^\dagger_{p\tau\sigma}(\mathbf{R})c_{p+1\tau\sigma}(\mathbf{R}) + \text{H.c.}]. \tag{3}$$

Here, U sets the overall interaction strength, $\mathbf{R}$ labels the position of a hexagon, and p labels the six sites in each hexagon (see Fig. 1). The factor of $1/3$ in $Q(\mathbf{R})$ accounts for the triple

counting, and $\tau = \pm 1$ ($\sigma = \uparrow, \downarrow$) is the valley (spin) degree of freedom of the Wannier orbitals represented by the operators $c_{p\tau\sigma}$. As illustrated in Figs. 1(a) and 1(b), the low-energy Wannier orbitals in MATBG exhibit an inherent nonlocality where, instead of the usual exponentially localized, single-peak, wave function, an orbital centered at site p exhibits three symmetric peaks in the adjacent hexagon centers [73,74]. In Fig. 1(a) we depict the cluster charge interaction term $Q(\mathbf{R})$, a standard charge density term apart from the nonlocal wave function distribution. Thus, the contribution to $H_{\rm int}$ from $Q^2(\mathbf{R})$ is analogous to a hexagon-centered density-density Hubbard term containing on-site and up to third-nearest-neighbor interactions in the projected model orbitals.

The assisted-hopping interaction term $T(\mathbf{R})$ is schematically shown in Fig. 1(b), where horizontal blue (vertical red) lines indicate the density distribution of a Wannier orbital residing at the blue (red) honeycomb site. While the total overlap of the two neighboring orbitals must be zero because of orthogonality requirements, the overlap within a single hexagon [highlighted in green in Fig. 1(b)] can be finite due to the Wannier obstruction preventing all symmetries from being implemented locally [38]. Thus, this term is topological in nature. In Ref. [38] the authors found that the overlap integral $\alpha \sim 1/3$, yielding comparable interaction strengths for the $Q(\mathbf{R})$ and $T(\mathbf{R})$ terms. The assisted-hopping interactions are pivotal to all results presented in this paper.

The kinetic terms of the Hamiltonian were proposed, e.g., in Refs. [73–75]. The effective tight-binding model is defined on the AB/BA honeycomb lattice of the moiré superlattice and includes nearest-neighbor (NN) as well as complex fifth-NN hopping. The model has eight narrow bands reflecting the spin, valley, and sublattice degrees of freedom. In the notation of Eq. (1), the minimal tight-binding kinetic part reads

$$H_0 = \sum_{\mathbf{R}} \sum_{p,\tau,\sigma} \Big[-\frac{\mu}{3} c^\dagger_{p\tau\sigma}(\mathbf{R}) c_{p\tau\sigma}(\mathbf{R}) + t_1 e^{(-1)^{p-1} i\tau\phi} c^\dagger_{p\tau\sigma}(\mathbf{R}) c_{p+1\tau\sigma}(\mathbf{R}) + \frac{1}{3} \sum_{\mathbf{R}'} [(t_2 - \tau i t_2') c^\dagger_{p\tau\sigma}(\mathbf{R}) c_{p\tau\sigma}(\mathbf{R}') + \text{H.c.}] \Big], \tag{4}$$

where μ is the chemical potential, t_1 is the NN hopping amplitude, and the phase factor $e^{(-1)^{p-1} i\tau\phi}$ arises from a convenient gauge transformation ensuring $\alpha \in \mathbb{R}$ in Eq. (3) [38]. In the last term $\mathbf{R}'$ refers to three next-NN hexagons to $\mathbf{R}$ related by C_3 symmetry. As the site indices p within $\mathbf{R}$ and $\mathbf{R}'$ are identical, these terms are fifth-NN hoppings with real (t_2) and imaginary (t_2') hopping amplitudes, respectively [see Fig 1(c)].

The validity of mean-field approaches in describing interacting electrons in moiré flat bands is questionable. However, as mentioned above, HF theory has been rather widely applied and has provided insight into the possible ordered phases. Additionally, relevant for the present model, HF results were shown to agree surprisingly well with QMC simulations at charge neutrality. Motivated by these previous results, we proceed by performing an unrestricted HF decoupling of Eq. (1), yielding

$$H^{\rm HF}_{\rm int} = U \sum_{\mathbf{R}} \left(\bar{n}(\mathbf{R})[Q(\mathbf{R}) + T(\mathbf{R})] - \sum_{\rm all} \left[\sum_{n,m} \alpha_n(p') \alpha_m(p) \langle c^\dagger_{p'+n\tau'\sigma'} c_{p+m\tau\sigma} \rangle \right] c^\dagger_{p\tau\sigma} c_{p'\tau'\sigma'} \right), \tag{5}$$

with

$$\bar{n}(\mathbf{R}) = \sum_{p',\tau',\sigma'} \left(\frac{1}{3} \langle c^\dagger_{p'\tau'\sigma'} c_{p'\tau'\sigma'} \rangle + \alpha(-1)^{p'} [\langle c^\dagger_{p'\tau'\sigma'} c_{p'+1\tau'\sigma'} \rangle + \langle c^\dagger_{p'+1\tau'\sigma'} c_{p'\tau'\sigma'} \rangle] \right). \tag{6}$$

Here, $\sum_{\rm all} = \sum_{p,p'} \sum_{\tau,\tau'} \sum_{\sigma,\sigma'}$, and $n, m \in \{-1, 0, 1\}$. We have suppressed the $\mathbf{R}$ dependence of the operators for clarity and defined $\alpha(p) \equiv (\alpha_{-1}(p), \alpha_0(p), \alpha_1(p)) = (\alpha(-1)^{p-1}, 1/3, \alpha(-1)^p)$. Note from the definition of $\alpha(p)$ that setting $\alpha \neq 0$ inevitably introduces nonlocality in the Fock exchange terms since, e.g., NNN hopping $c^\dagger_p c_{p'=p+2}$ will contain contributions from on-site mean fields $\langle c^\dagger_{p+2-1} c_{p+1} \rangle$ for $n = -1$ and $m = 1$.

The unrestricted HF decoupling leading to Eq. (5) allows for spontaneous breaking of all symmetries, including translational invariance, yielding a total of $R_{\rm tot}/3 \times 24 \times 24 \sim O(10^5)$ different mean fields to be solved for typical systems sizes with a total number of hexagons $R_{\rm tot} = 300$ [see Fig. 3(d) below]. The resulting decoupled Hamiltonian, $H = H_0 + H^{\rm HF}_{\rm int}$, is solved self-consistently with unbiased initial conditions. For the results reported in this paper, we have defined the convergence criterion to be $\sum_{n=1}^{N} |E_n(m-1) - E_n(m)| < N \times 10^{-10} t_1$, where m denotes an iteration counter and $N = R_{\rm tot}/3 \times 24 \times 24$ is the total number of eigenenergies E_n. Guided by Refs. [38,75], we fix $\{t_1, t_2, t_2', \phi, \alpha\} = \{1.0, 0.025, 0.1, 0.743\pi, 0.23\}$ while the filling is controlled by varying μ during the iterations until the desired filling factor is reached. Further technical details of the HF procedure can be found in Appendix C of Ref. [65]. As usual, we denote the filling factor by ν, which is related to the carrier density n by $\nu = 4n/n_s$, where n_s is the density of the filled moiré superlattice flat bands. The temperature is set to $T = 2.5 \times 10^{-5} t_1$, representative of the $T = 0$ limit, in all computations below.

III. RESULTS

A. Phase diagram: Homogeneous phases

We start by presenting a main result of the paper in Fig. 2: the full phase diagram as a function of interaction strength at all integer fillings. Focusing first on homogeneous phases found at sufficiently large interaction strengths U/W, the

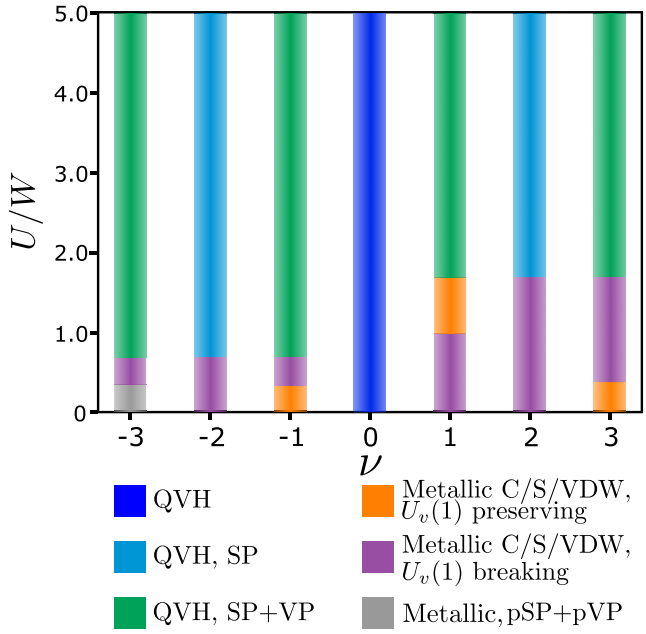

FIG. 2. Phase diagram indicating the preferred order at integer filling factors as a function of interaction strength U/W, where $W = 6t_1$ is the bare bandwidth. Charge neutrality features only a QVH phase in this range of interactions. The other integer fillings exhibit different ferromagnetic order with spin/valley polarization beyond a certain interaction threshold. Below this critical interaction value, all nonzero integer fillings prefer different inhomogeneous metallic phases. Note that the metallic phase marked in gray at $\nu = -3$ is only partially spin and valley polarized (pSP, pVP).

emergent orders are (i) QVH order consisting of imaginary next-nearest-neighbor (iNNN) hopping, $\mathrm{Im}\langle c^\dagger_{p\tau\sigma} c_{p+2\tau\sigma}\rangle \neq 0$ [see Fig. 3(a)], (ii) fully spin polarized (SP) order characterized by ferromagnetic on-site mean fields, $\langle n_\uparrow\rangle - \langle n_\downarrow\rangle = 1, 2$, with $\langle n_\sigma\rangle = \frac{1}{3}\sum_{p\tau}\langle c^\dagger_{p\tau\sigma} c_{p\tau\sigma}\rangle$, i.e., an excess of either one or two spin-up electrons per moiré unit cell, and (iii) fully valley polarized (VP) order defined by $\langle n_{+1}\rangle - \langle n_{-1}\rangle = \pm 1$, with $\langle n_{\pm 1}\rangle = \frac{1}{3}\sum_{p\sigma}\langle c^\dagger_{p,\pm 1,\sigma} c_{p,\pm 1,\sigma}\rangle$.

Despite the rich variety of possible symmetry breaking in MATBG, we find QVH order to be present in the ground state across all integer fillings in a wide range of interaction strengths. In Fig. 2 the QVH phase is indicated by dark blue when it is not symmetry breaking, light blue when it coexists with the spin polarization, and green when it coexists with both spin and valley polarization. At charge neutrality, the QVH phase is induced even for very small interaction strengths, in agreement with Ref. [65], whereas at all nonzero integer fillings stabilization of the QVH phase requires a critical value of U/W. The emergent iNNN hopping leads to an insulating gap as expected from the Haldane model [76]. The QVH phase preserves the $U_v(1)$ symmetry, yielding a total of four decoupled sectors (valley × spin) of the Haldane bands. The direction of the iNNN hopping is dictated by the valley flavor alone [see Fig. 3(a)]. Finally, we note that both H_0 and H_{int} break particle-hole symmetry, resulting in a significant particle-hole asymmetry of the phase diagram in Fig. 2 [65].

B. Resulting band structure

We turn now to the band structure associated with the homogeneous phases present in the phase diagram of Fig. 2. The left panel in Fig. 3(b) shows the bare bands, exhibiting the well-known semimetallic Dirac dispersion [73–75]. The middle and right panels of Fig. 3(b) display the band structure at $U/W = 2.0$ and $\nu = -2, 2$, respectively. From the renormalized bands at $\nu = -2$ it is evident that the interactions shift the minima of the occupied bands from Γ_{m} to K_{m} (K'_{m}). The shift is caused by the assisted-hopping interactions, which, as mentioned in the previous section, introduce longer-range hoppings, leading to a nontrivial structure of H_{int}. Combining this interaction-originated structure with the bare bands leads to distinct renormalization of the four lower and upper bands, respectively. At weak interactions ($U/W \lesssim 1.0$) the renormalization of the four lower bands suppresses the bandwidth significantly, followed by the inversion evident in the middle panel of Fig. 3(b) at larger interaction strength. On the contrary, since the upper four bands exhibit a momentum dependence similar to H_{int}, the interactions will enhance the bandwidth of these bands for all interaction strengths, leading to reduced gap sizes as well as larger critical U/W for all $\nu > 0$ [see the right panel of Fig. 3(b)].

By further inspection of Fig. 3(b) several similarities between the band structures at $\nu = -2$ and 2 can be identified. Both structures exhibit significant energy gaps in two out of four Haldane sectors [red sectors in Fig. 3(b)], in agreement with their respective fillings. However, more strikingly, we note that these two sectors are identical at the two different fillings. As such, the sole qualitative discrepancy between $\nu = -2$ and 2 is whether the remaining two gapless sectors [black sectors in Fig. 3(b)] are empty ($\nu = -2$) or full ($\nu = 2$). The similarity between the QVH band structures in Fig. 3(b) serves as an example of the general interpretation of the QVH phases across all integer fillings, as illustrated in Fig. 3(c). At $\nu = -4$ the system consists of four empty, gapless, and decoupled band sectors characterized by the valley and spin degrees of freedom $\{\tau, \sigma\}$. Doping the narrow bands to the first commensurate filling ($\nu = -3$) results in an accumulation of all electrons into a single flavor. This accumulation is energetically favored because it allows for a gap opening in the corresponding band sector at the expense of spontaneously generated loop currents (i.e., iNNN hoppings). Upon further electron filling, the mechanism repeats at each integer filling where a gap is introduced in one of the (previously gapless) sectors, until all four flavors are fully gapped at charge neutrality ($\nu = 0$). Increasing the electron density further, the mechanism reverses such that at each integer filling, an additional conduction band is fully occupied. Since all anomalous hopping terms (i.e., spin/valley flipping hoppings) vanish, the electrons in the fully occupied sectors are effectively blocked, leading to a gap closing because iNNN hopping is prohibited. We attribute this behavior to be related to the cascade of transitions seen experimentally [25–27].

C. Topology and edge states of the insulating phases

The emergence of loop currents and spin polarization naturally leads to a consideration of time-reversal symmetry breaking (TRSB). As all four flavor sectors remain decoupled

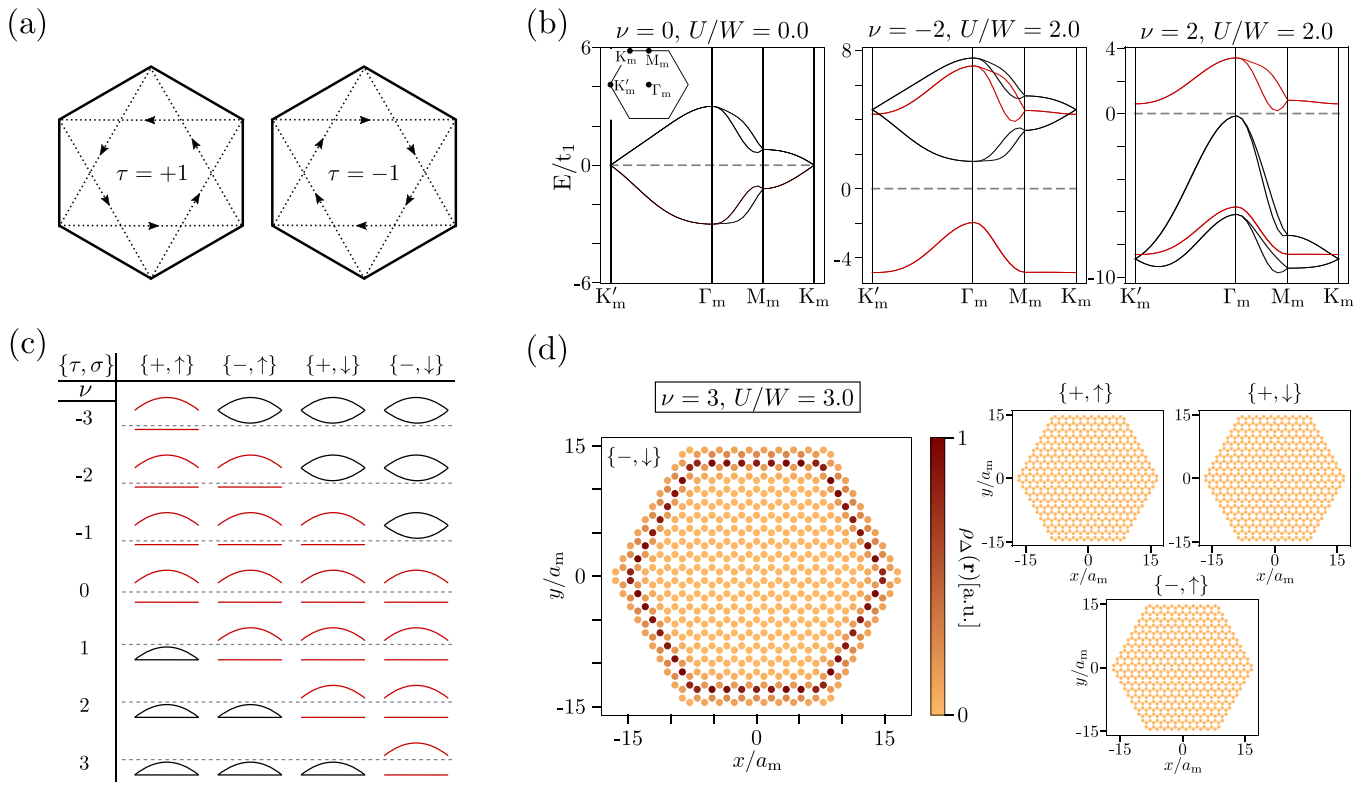

FIG. 3. (a) Illustration of emergent imaginary NNN hoppings in the QVH phases. The arrow direction indicates the direction of the corresponding loop currents dictated by the valley flavor. (b) Bare bands at charge neutrality (left panel) and renormalized bands at interaction strength $U/W = 2.0$ for $\nu = -2$ (middle panel) and $\nu = +2$ (right panel). Gapless (gapped) band sectors are marked in black (red). The inset in the left panel shows the miniature Brillouin zone. (c) Schematic of successive filling of bands and resulting gap opening or closing at all integer filling factors of the four decoupled Haldane sectors. Each sector is characterized by the spin and valley flavor $\{\tau, \sigma\}$. (d) In-gap local density of states $\rho_\Delta(\mathbf{r})$ of the spin- and valley-polarized QVH phase at $\nu = 3.0$ and $U/W = 3.0$. A single topologically protected edge state is present in the only remaining gapped sector $\{-, \downarrow\}$. The results in (d) are computed by opening the boundaries in a result converged with periodic boundary conditions.

in the QVH phases throughout the entire doping range, it is evident that the QVH order is accompanied by flavor polarization at all nonzero integer fillings. Specifically, all even filling factors ($\nu = \pm 2$) are spin polarized, while all odd filling factors ($\nu = \pm 1, \pm 3$) exhibit both valley and spin polarization. Thus, time-reversal symmetry is spontaneously broken in the QVH phases at all nonzero integer filling factors. Since TRSB is the crucial element to obtain nontrivial topological bands in the Haldane model, it is reasonable to assume that the QVH phases discussed here also exhibit nontrivial topology. To verify this explicitly, we compute the Chern numbers at all integer fillings by evaluating the usual momentum integral

$$C_n = \frac{1}{2\pi} \int_{mBZ} d^2\mathbf{k}\, \mathrm{Tr}[\Omega^n(\mathbf{k})], \tag{7}$$

where the Berry curvature is defined by

$$\Omega^n(\mathbf{k}) = iP_n(\mathbf{k})\big[\partial_{k_x} P_n(\mathbf{k}), \partial_{k_y} P_n(\mathbf{k})\big] \tag{8}$$

and P_n is the projector to the corresponding band defined by the flavor sector and particle or hole character. The resulting Chern numbers are $C_n = \pm 1$ (∓ 1) for the valence (conduction) band in $\tau = \pm 1$ insulating sectors. The invariants are independent of spin direction, in agreement with the purely valley defined hopping direction depicted in Fig. 3(a). Not surprisingly, the nongapped, fully occupied sectors yield $C_n = 0$ for both bands, which is verified by introducing a perturbative splitting prior to the Chern number computation. Thus, all half-filled sectors host a single edge state, while fully occupied sectors do not. An example of this property is shown in Fig. 3(d), which displays the in-gap local density of states $\rho_\Delta(\mathbf{r})$ for all four sectors in the QVH phase at $\nu = 3$. As the propagation direction of the edge states is set by the valley degree of freedom, these findings yield quantum anomalous Hall phases, i.e., a nonzero total Chern number, for all valley polarized QVH phases, that is, for all odd-integer fillings.

D. Phase diagram: Inhomogeneous phases

As indicated in Fig. 2, inhomogeneous metallic phases exist at all finite integer filling factors in the regime of low to intermediate interaction strengths, as expected for weak-coupling approaches. In Fig. 2 these phases are indicated in either orange [$U_v(1)$ preserving] or purple [$U_v(1)$ breaking] as the gapless and inhomogeneous properties are common to all. However, the flavor order degree of freedom as well as the specific ordering vector(s) are found to depend on the

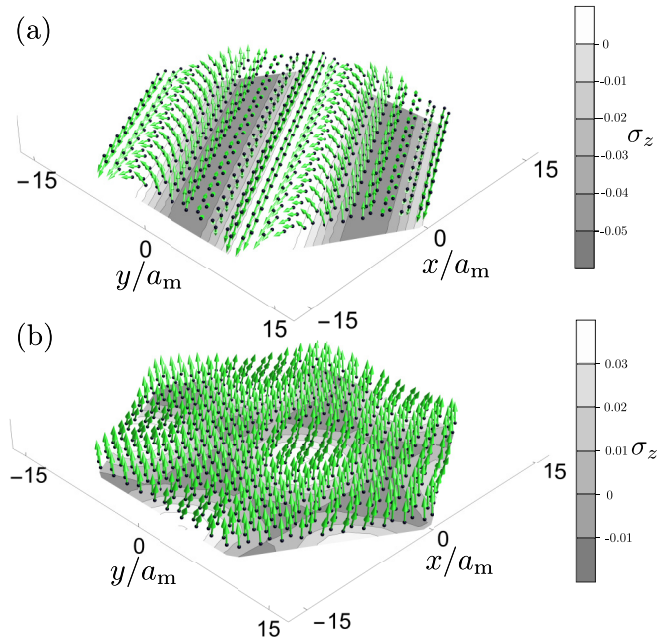

FIG. 4. Examples of inhomogeneous metallic spin-ordered phases for (a) $U/W = 0.5$ and (b) $U = 0.33$ at $\nu = 1.0$. Contours in gray show the local z component of the spin, i.e., $\sigma_z = \frac{1}{2}\sum_\tau(\langle n_{i\tau\uparrow}\rangle - \langle n_{i\tau\downarrow}\rangle)$. The structure in (a) breaks C_3 symmetry, and a single ordering vector has condensed along all three directions of the Bloch sphere. The structure shown in (b) preserves C_3 symmetry, and three symmetry-related ordering vectors have condensed in all three directions.

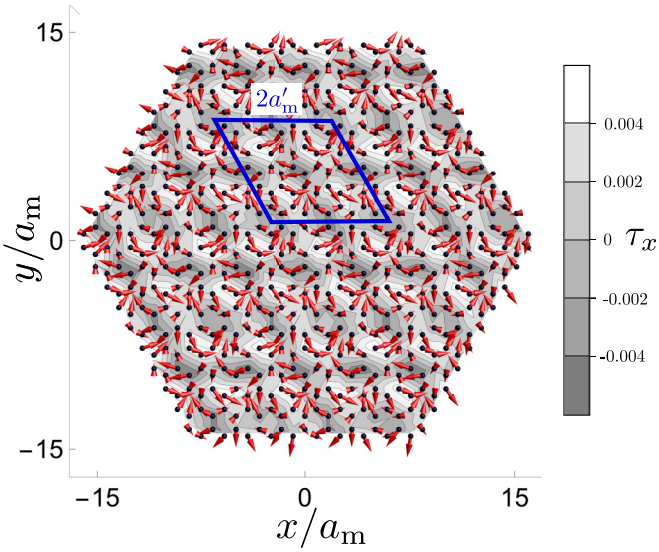

FIG. 5. Example of inhomogeneous metallic valley-ordered phase for $U/W = 0.33$ at $\nu = 2.0$. Contours in gray show the local x component of the valley order, i.e., $\tau_x = \sum_\sigma \mathrm{Re}(\langle c^\dagger_{i,+,\sigma} c_{i,-,\sigma}\rangle + \langle c^\dagger_{i,-,\sigma} c_{i,+,\sigma}\rangle)$. The order is restricted to the xy plane of the valley Bloch sphere, and the unit cell is enlarged to $a'_m = 2.5a_m$, as indicated by the blue rhombus.

particular filling factor and interaction strength. The variety of phases identified in the low to intermediate interaction regime implies a plethora of (near-)degenerate states in this region. This combined with the impact of finite size effects in self-consistent computations of inhomogeneous ground states causes significant convergence difficulties, and the notion of simulations trapped in local minima in the extensive phase space cannot be dismissed. Nonetheless, the breaking of translation symmetry and the gapless energy spectrum are highly robust features across all nonzero integer fillings at these interaction strengths.

Examples of typical inhomogeneous phases are shown in Fig. 4. Figure 4(a) displays the spin structure of the converged result at $U/W = 0.5$ and $\nu = 1$, where a single ordering vector has condensed in all three directions of the Bloch sphere. The spin modulations in the three directions have relative phase shifts resulting in a spin spiral with a net relative magnetization of $\langle S^z_i\rangle/\langle|\mathbf{S}_i|\rangle = 0.24$ per site. For lower interactions $U/W = 0.33$ at $\nu = 1$, the ground state exhibits the spin pattern shown in Fig. 4(b) with a net relative magnetization of $\langle S^z_i\rangle/\langle|\mathbf{S}_i|\rangle = 0.97$ per site accompanied by C_3-preserving ordering vectors for each spin direction.

Figure 5 shows an example of a valley-ordered phase exhibited at weak coupling at $\nu = 2.0$. This phase is characterized by spatially modulating intervalley coherence, breaking both translation and $U_v(1)$ symmetries. The direction of this modulating intervalley coherence is restricted to the xy plane of the valley Bloch sphere; that is, the occupation of the two valleys is identical. In this case, the order is defined by C_3-related vectors of length $|\mathbf{q}_i| = 0.4|\mathbf{G}_m|$, where $\mathbf{G}_m$ denotes the reciprocal lattice vectors of the moiré Brillouin zone (mBZ). Interestingly, a modulated intervalley coherence phase was also recently explored within HF studies of the Bistritzer-MacDonald model, and it was found to be the preferred ground state across all nonzero integer fillings in the presence of a small C_3-breaking heterostrain [67,69]. There, access to the graphene scale has identified this order as an incommensurate Kekulé pattern.

Finally, we stress that while the inhomogeneous phases discussed above are driven by a single degree of freedom, the order is generally inherited in the remaining degrees of freedom. An example is the negligible, yet finite, spin order ($\langle|\mathbf{S}_i|\rangle = 0.002$ per site) in the valley-ordered phase depicted in Fig. 5.

E. Modulated phases at half-integer filling

Recently, Bhowmik *et al.* [24] studied MATBG proximitized by a layer of WSe_2 and reported distinct features in magnetotransport and thermoelectricity consistent with ordered phases setting in at half-integer filling factors, $\nu = \pm 0.5$ and $\nu = \pm 3.5$. These results were interpreted in terms of correlation-induced modulated spin- and charge density wave order with doubled unit cell order at the moiré scale. We computed the mean fields at $\nu = \pm 0.5$ and show the resulting intervalley coherent order at $\nu = -0.5$ and $U/W = 0.33$ in Fig. 6. As can be seen, the order is similar to the intervalley coherence spiral shown in Fig. 5 with an additional breaking of C_3 symmetry. The intervalley order is restricted to the xy plane of the valley Bloch sphere, and we find a well-defined ordering vector of length $|\mathbf{q}| = 0.2|\mathbf{G}_m|$ with a relative phase

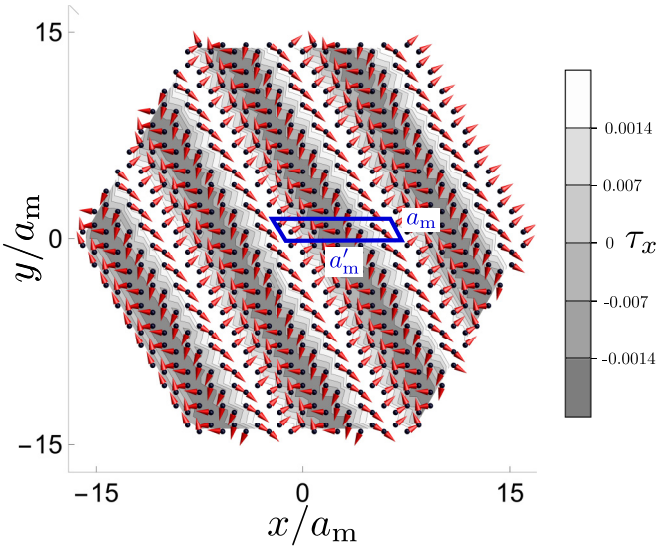

FIG. 6. Example of inhomogeneous metallic valley-ordered phase for $U/W = 0.33$ at $\nu = -0.5$. Contours in gray show the local x component of the valley order, i.e., $\tau_x = \sum_\sigma \mathrm{Re}(\langle c^\dagger_{i,+,\sigma} c_{i,-,\sigma}\rangle + \langle c^\dagger_{i,-,\sigma} c_{i,+,\sigma}\rangle)$. The order is restricted to the xy plane of the valley Bloch sphere defined by a single ordering vector of length $|\mathbf{q}| = 0.2|\mathbf{G}_{\mathrm{m}}|$ ($a'_{\mathrm{m}} = 5a_{\mathrm{m}}$) with a relative phase between the x and y directions yielding an intervalley coherent spiral.

between the x and y directions, yielding an intervalley coherent spiral along $\mathbf{q}$. Similar to the inhomogeneous phases discussed in the previous section, the phase shown in Fig. 6 is metallic.

For larger interaction strengths at half-integer filling $\nu = \pm 0.5$ the ground states remain periodically modulated metallic phases dominated by order in the valley degree of freedom. For example, at $U/W = 1.0$ and $\nu = -0.5$ the order is a modulated valley polarization preserving $U_v(1)$ symmetry, while intervalley coherence is present in the valley-ordered state at $\nu = +0.5$. However, it should be noted that, at these higher interaction strengths, significant order is also present in the spin degree of freedom with magnitudes smaller than but comparable to the valley order. Thus, the appearance of modulated ordered phases is a robust feature also at half-integer fillings of the current model, and this may be related to the unusual magnetotransport features detected in recent experiments [24].

IV. DISCUSSION AND CONCLUSIONS

We have performed an unrestricted self-consistent HF study of a moiré lattice model designed for MATBG with both local and nonlocal interactions truncated to NN sites, obtained from Wannier projected Coulomb repulsion, and mapped out the preferred ordered phases as a function of interaction strength and the moiré flat-band filling factor. This model proposed by Kang and Vafek was previously addressed, e.g., from a strong-coupling perspective and also studied via numerical methods, including QMC simulations and density matrix renormalization group (DMRG) calculations [38,40,60,65]. For example, Ref. [60] recently studied the model in the flat-band, flavor-polarized limit at half filling using a DMRG approach (corresponding to half filling of one of the four decoupled band sectors discussed in Sec. III B with $H_0 = 0$). The study reports a first-order phase transition from a stripe charge density wave phase to the QVH phase at a critical assisted-hopping interaction of $\alpha_c/U \approx 0.12$. Interestingly, the authors found a remarkably low von Neumann entropy of the QVH phase and argued, therefore, that a similar ground state should be well captured by a self-consistent mean-field description, a conjecture consistent with the results presented here even in the non-flat-band limit without assuming flavor polarization.

Furthermore, previous HF studies of the Kang-Vafek model restricted to charge neutrality but including a NN tight-binding hopping term in the Hamiltonian obtained the QVH phase and were shown to agree well with QMC simulations [65]. Here, we have extended such HF studies to include other electron filling factors and explored the resulting preferred ordered phases. As seen from Fig. 2, for interaction strengths that are large enough we obtain ferromagnetic spin/valley polarized order coexisting with the QVH phase. This, in turn, gives rise to a particular filling dependence of the moiré bands with Chern insulator phases at integer filling factors and the presence of quantum anomalous Hall effect at odd filling factors. Thus far, experimental efforts have revealed a multitude of Chern insulator phases in MATBG under the application of an external magnetic field [20–23]; however, it has proved challenging to observe topological signatures of the correlated insulators in the absence of external fields, most likely due to sample imperfections [18,19]. Nevertheless, two observations of (nearly) quantized anomalous Hall effects at $\nu = +1, +3$ alongside a detailed inverse compressibility study down to zero field at $\nu = +1, +2, +3$ were published recently [17,18,22]. Interestingly, while many reports on field-stabilized Chern insulators in MATBG found sequences of $\{C, \nu\} = \{\pm 4, 0\}, \{\pm 3, \pm 1\}, \{\pm 2, \pm 2\}, \{\pm 1, \pm 3\}$, the zero-field Chern insulators at $\nu = +1, +3$ ($\nu = +2$) have quantizations of $|C| = 1$ ($C = 0$), in agreement with the results presented here.

At weak to intermediate interaction strengths $U/W \lesssim 1$, the preferred ground states become inhomogeneous with density wave order in spin/valley degrees of freedom. Similar inhomogeneous phases are found at certain half-integer filling factors, which appears to be consistent with recent experimental reports of ordered spatially modulated phases at certain half-integer filling factors [24]. We stress that the modulated phases discussed here are intrinsic, i.e., generated solely by the interactions. In actual samples external inhomogeneities from, e.g., strain or twist-angle variations will lead to additional spatial variations of pinned order, possibly producing a mosaic of regions featuring different topological properties [19]. Inclusion of such effects and a more detailed comparison to experiments in terms of the derived spectral properties and transport coefficients are beyond the scope of the current work. Here, we have focused on mapping out the filling dependence of the preferred ordered phases of the present moiré lattice model. This already exhibits a plethora of different phases, some of which constitute fascinating examples of interaction-driven nontrivial topological states of matter.

ACKNOWLEDGMENTS

We acknowledge useful discussions with E. Berg, M. H. Christensen, R. M. Fernandes, M. Geier, J. Kang, Z.-Y. Meng, and G. Wagner. C.N.B. acknowledges support from the Danish National Committee for Research Infrastructure (NUFI) through the ESS-Lighthouse Q-MAT.

[1] Y. Cao, V. Fatemi, A. Demir, S. Fang, S. L. Tomarken, J. Y. Luo, J. D. Sanchez-Yamagishi, K. Watanabe, T. Taniguchi, E. Kaxiras, R. C. Ashoori, and P. Jarillo-Herrero, Correlated insulator behaviour at half-filling in magic-angle graphene superlattices, Nature (London) **556**, 80 (2018).

[2] Y. Cao, V. Fatemi, S. Fang, K. Watanabe, T. Taniguchi, E. Kaxiras, and P. Jarillo-Herrero, Unconventional superconductivity in magic-angle graphene superlattices, Nature (London) **556**, 43 (2018).

[3] E. Y. Andrei and A. H. MacDonald, Graphene bilayers with a twist, Nat. Mater. **19**, 1265 (2020).

[4] L. Balents, C. R. Dean, D. K. Efetov, and A. F. Young, Superconductivity and strong correlations in moiré flat bands, Nat. Phys. **16**, 725 (2020).

[5] J. M. B. Lopes dos Santos, N. M. R. Peres, and A. H. Castro Neto, Graphene Bilayer with a Twist: Electronic Structure, Phys. Rev. Lett. **99**, 256802 (2007).

[6] E. Suárez Morell, J. D. Correa, P. Vargas, M. Pacheco, and Z. Barticevic, Flat bands in slightly twisted bilayer graphene: Tight-binding calculations, Phys. Rev. B **82**, 121407(R) (2010).

[7] R. Bistritzer and A. H. MacDonald, Moiré bands in twisted double-layer graphene, Proc. Natl. Acad. Sci. USA **108**, 12233 (2011).

[8] X. Lu, P. Stepanov, W. Yang, M. Xie, M. A. Aamir, I. Das, C. Urgell, K. Watanabe, T. Taniguchi, G. Zhang, A. Bachtold, A. H. MacDonald, and D. K. Efetov, Superconductors, orbital magnets and correlated states in magic-angle bilayer graphene, Nature (London) **574**, 653 (2019).

[9] M. Yankowitz, S. Chen, H. Polshyn, Y. Zhang, K. Watanabe, T. Taniguchi, D. Graf, A. F. Young, and C. R. Dean, Tuning superconductivity in twisted bilayer graphene, Science **363**, 1059 (2019).

[10] Y. Xie, B. Lian, B. Jäck, X. Liu, C.-L. Chiu, K. Watanabe, T. Taniguchi, B. A. Bernevig, and A. Yazdani, Spectroscopic signatures of many-body correlations in magic-angle twisted bilayer graphene, Nature (London) **572**, 101 (2019).

[11] A. Kerelsky, L. J. McGilly, D. M. Kennes, L. Xian, M. Yankowitz, S. Chen, K. Watanabe, T. Taniguchi, J. Hone, C. Dean, A. Rubio, and A. N. Pasupathy, Maximized electron interactions at the magic angle in twisted bilayer graphene, Nature (London) **572**, 95 (2019).

[12] Y. Jiang, X. Lai, K. Watanabe, T. Taniguchi, K. Haule, J. Mao, and E. Y. Andrei, Charge order and broken rotational symmetry in magic-angle twisted bilayer graphene, Nature (London) **573**, 91 (2019).

[13] P. Stepanov, I. Das, X. Lu, A. Fahimniya, K. Watanabe, T. Taniguchi, F. H. L. Koppens, J. Lischner, L. Levitov, and D. K. Efetov, Untying the insulating and superconducting orders in magic-angle graphene, Nature (London) **583**, 375 (2020).

[14] Y. Saito, J. Ge, K. Watanabe, T. Taniguchi, and A. F. Young, Independent superconductors and correlated insulators in twisted bilayer graphene, Nat. Phys. **16**, 926 (2020).

[15] J. M. Park, Y. Cao, K. Watanabe, T. Taniguchi, and P. Jarillo-Herrero, Flavour Hund's coupling, Chern gaps and charge diffusivity in moiré graphene, Nature (London) **592**, 43 (2021).

[16] A. L. Sharpe, E. J. Fox, A. W. Barnard, J. Finney, K. Watanabe, T. Taniguchi, M. A. Kastner, and D. Goldhaber-Gordon, Emergent ferromagnetism near three-quarters filling in twisted bilayer graphene, Science **365**, 605 (2019).

[17] M. Serlin, C. L. Tschirhart, H. Polshyn, Y. Zhang, J. Zhu, K. Watanabe, T. Taniguchi, L. Balents, and A. F. Young, Intrinsic quantized anomalous Hall effect in a moiré heterostructure, Science **367**, 900 (2020).

[18] P. Stepanov, M. Xie, T. Taniguchi, K. Watanabe, X. Lu, A. H. MacDonald, B. A. Bernevig, and D. K. Efetov, Competing Zero-Field Chern Insulators in Superconducting Twisted Bilayer Graphene, Phys. Rev. Lett. **127**, 197701 (2021).

[19] S. Grover, M. Bocarsly, A. Uri, P. Stepanov, G. Di Battista, I. Roy, J. Xiao, A. Y. Meltzer, Y. Myasoedov, K. Pareek, K. Watanabe, T. Taniguchi, B. Yan, A. Stern, E. Berg, D. K. Efetov, and E. Zeldov, Chern mosaic and Berry-curvature magnetism in magic-angle graphene, Nat. Phys. **18**, 885 (2022).

[20] K. P. Nuckolls, M. Oh, D. Wong, B. Lian, K. Watanabe, T. Taniguchi, B. A. Bernevig, and A. Yazdani, Strongly correlated Chern insulators in magic-angle twisted bilayer graphene, Nature (London) **588**, 610 (2020).

[21] S. Wu, Z. Zhang, K. Watanabe, T. Taniguchi, and E. Y. Andrei, Chern insulators, Van Hove singularities and topological flat bands in magic-angle twisted bilayer graphene, Nat. Mater. **20**, 488 (2021).

[22] A. T. Pierce, Y. Xie, J. M. Park, E. Khalaf, S. H. Lee, Y. Cao, D. E. Parker, P. R. Forrester, S. Chen, K. Watanabe, T. Taniguchi, A. Vishwanath, P. Jarillo-Herrero, and A. Yacoby, Unconventional sequence of correlated Chern insulators in magic-angle twisted bilayer graphene, Nat. Phys. **17**, 1210 (2021).

[23] I. Das, X. Lu, J. Herzog-Arbeitman, Z.-D. Song, K. Watanabe, T. Taniguchi, B. A. Bernevig, and D. K. Efetov, Symmetry-broken Chern insulators and Rashba-like Landau-level crossings in magic-angle bilayer graphene, Nat. Phys. **17**, 710 (2021).

[24] S. Bhowmik, B. Ghawri, N. Leconte, S. Appalakondaiah, M. Pandey, P. S. Mahapatra, D. Lee, K. Watanabe, T. Taniguchi, J. Jung, A. Ghosh, and U. Chandni, Broken-symmetry states at half-integer band fillings in twisted bilayer graphene, Nat. Phys. **18**, 639 (2022).

[25] U. Zondiner, A. Rozen, D. Rodan-Legrain, Y. Cao, R. Queiroz, T. Taniguchi, K. Watanabe, Y. Oreg, F. von Oppen, A. Stern, E. Berg, P. Jarillo-Herrero, and S. Ilani, Cascade of phase

transitions and Dirac revivals in magic-angle graphene, Nature (London) **582**, 203 (2020).

[26] D. Wong, K. P. Nuckolls, M. Oh, B. Lian, Y. Xie, S. Jeon, K. Watanabe, T. Taniguchi, B. A. Bernevig, and A. Yazdani, Cascade of electronic transitions in magic-angle twisted bilayer graphene, Nature (London) **582**, 198 (2020).

[27] Y. Choi, H. Kim, C. Lewandowski, Y. Peng, A. Thomson, R. Polski, Y. Zhang, K. Watanabe, T. Taniguchi, J. Alicea, and S. Nadj-Perge, Interaction-driven band flattening and correlated phases in twisted bilayer graphene, Nat. Phys. **17**, 1375 (2021).

[28] G. Chen, L. Jiang, S. Wu, B. Lyu, H. Li, B. L. Chittari, K. Watanabe, T. Taniguchi, Z. Shi, J. Jung, Y. Zhang, and F. Wang, Evidence of a gate-tunable Mott insulator in a trilayer graphene moiré superlattice, Nat. Phys. **15**, 237 (2019).

[29] G. Chen, A. L. Sharpe, P. Gallagher, I. T. Rosen, E. J. Fox, L. Jiang, B. Lyu, H. Li, K. Watanabe, T. Taniguchi, J. Jung, Z. Shi, D. Goldhaber-Gordon, Y. Zhang, and F. Wang, Signatures of tunable superconductivity in a trilayer graphene moiré superlattice, Nature (London) **572**, 215 (2019).

[30] Y. Cao, D. Rodan-Legrain, O. Rubies-Bigorda, J. M. Park, K. Watanabe, T. Taniguchi, and P. Jarillo-Herrero, Tunable correlated states and spin-polarized phases in twisted bilayer–bilayer graphene, Nature (London) **583**, 215 (2020).

[31] C. Shen, Y. Chu, Q. Wu, N. Li, S. Wang, Y. Zhao, J. Tang, J. Liu, J. Tian, K. Watanabe, T. Taniguchi, R. Yang, Z. Y. Meng, D. Shi, O. V. Yazyev, and G. Zhang, Correlated states in twisted double bilayer graphene, Nat. Phys. **16**, 520 (2020).

[32] X. Liu, Z. Hao, E. Khalaf, J. Y. Lee, Y. Ronen, H. Yoo, D. Haei Najafabadi, K. Watanabe, T. Taniguchi, A. Vishwanath, and P. Kim, Tunable spin-polarized correlated states in twisted double bilayer graphene, Nature (London) **583**, 221 (2020).

[33] H. C. Po, L. Zou, A. Vishwanath, and T. Senthil, Origin of Mott Insulating Behavior and Superconductivity in Twisted Bilayer Graphene, Phys. Rev. X **8**, 031089 (2018).

[34] H. Isobe, N. F. Q. Yuan, and L. Fu, Unconventional Superconductivity and Density Waves in Twisted Bilayer Graphene, Phys. Rev. X **8**, 041041 (2018).

[35] A. Thomson, S. Chatterjee, S. Sachdev, and M. S. Scheurer, Triangular antiferromagnetism on the honeycomb lattice of twisted bilayer graphene, Phys. Rev. B **98**, 075109 (2018).

[36] J. F. Dodaro, S. A. Kivelson, Y. Schattner, X. Q. Sun, and C. Wang, Phases of a phenomenological model of twisted bilayer graphene, Phys. Rev. B **98**, 075154 (2018).

[37] M. Ochi, M. Koshino, and K. Kuroki, Possible correlated insulating states in magic-angle twisted bilayer graphene under strongly competing interactions, Phys. Rev. B **98**, 081102(R) (2018).

[38] J. Kang and O. Vafek, Strong Coupling Phases of Partially Filled Twisted Bilayer Graphene Narrow Bands, Phys. Rev. Lett. **122**, 246401 (2019).

[39] K. Seo, V. N. Kotov, and B. Uchoa, Ferromagnetic Mott State in Twisted Graphene Bilayers at the Magic Angle, Phys. Rev. Lett. **122**, 246402 (2019).

[40] Y. Da Liao, Z. Y. Meng, and X. Y. Xu, Valence Bond Orders at Charge Neutrality in a Possible Two-Orbital Extended Hubbard Model for Twisted Bilayer Graphene, Phys. Rev. Lett. **123**, 157601 (2019).

[41] Y.-H. Zhang, D. Mao, Y. Cao, P. Jarillo-Herrero, and T. Senthil, Nearly flat Chern bands in moiré superlattices, Phys. Rev. B **99**, 075127 (2019).

[42] T. M. R. Wolf, J. L. Lado, G. Blatter, and O. Zilberberg, Electrically Tunable Flat Bands and Magnetism in Twisted Bilayer Graphene, Phys. Rev. Lett. **123**, 096802 (2019).

[43] Z. Song, Z. Wang, W. Shi, G. Li, C. Fang, and B. A. Bernevig, All Magic Angles in Twisted Bilayer Graphene Are Topological, Phys. Rev. Lett. **123**, 036401 (2019).

[44] J. Liu, Z. Ma, J. Gao, and X. Dai, Quantum Valley Hall Effect, Orbital Magnetism, and Anomalous Hall Effect in Twisted Multilayer Graphene Systems, Phys. Rev. X **9**, 031021 (2019).

[45] A. O. Sboychakov, A. V. Rozhkov, A. L. Rakhmanov, and F. Nori, Many-body effects in twisted bilayer graphene at low twist angles, Phys. Rev. B **100**, 045111 (2019).

[46] L. Classen, C. Honerkamp, and M. M. Scherer, Competing phases of interacting electrons on triangular lattices in moiré heterostructures, Phys. Rev. B **99**, 195120 (2019).

[47] Y.-H. Zhang, D. Mao, and T. Senthil, Twisted bilayer graphene aligned with hexagonal boron nitride: Anomalous Hall effect and a lattice model, Phys. Rev. Res. **1**, 033126 (2019).

[48] N. Bultinck, E. Khalaf, S. Liu, S. Chatterjee, A. Vishwanath, and M. P. Zaletel, Ground State and Hidden Symmetry of Magic-Angle Graphene at Even Integer Filling, Phys. Rev. X **10**, 031034 (2020).

[49] D. V. Chichinadze, L. Classen, and A. V. Chubukov, Valley magnetism, nematicity, and density wave orders in twisted bilayer graphene, Phys. Rev. B **102**, 125120 (2020).

[50] N. Bultinck, S. Chatterjee, and M. P. Zaletel, Mechanism for Anomalous Hall Ferromagnetism in Twisted Bilayer Graphene, Phys. Rev. Lett. **124**, 166601 (2020).

[51] J. Kang and O. Vafek, Non-Abelian Dirac node braiding and near-degeneracy of correlated phases at odd integer filling in magic-angle twisted bilayer graphene, Phys. Rev. B **102**, 035161 (2020).

[52] L. Rademaker, I. V. Protopopov, and D. A. Abanin, Topological flat bands and correlated states in twisted monolayer-bilayer graphene, Phys. Rev. Res. **2**, 033150 (2020).

[53] T. Cea and F. Guinea, Band structure and insulating states driven by Coulomb interaction in twisted bilayer graphene, Phys. Rev. B **102**, 045107 (2020).

[54] M. Xie and A. H. MacDonald, Nature of the Correlated Insulator States in Twisted Bilayer Graphene, Phys. Rev. Lett. **124**, 097601 (2020).

[55] Y. Zhang, K. Jiang, Z. Wang, and F. Zhang, Correlated insulating phases of twisted bilayer graphene at commensurate filling fractions: A Hartree-Fock study, Phys. Rev. B **102**, 035136 (2020).

[56] C. Repellin, Z. Dong, Y.-H. Zhang, and T. Senthil, Ferromagnetism in Narrow Bands of Moiré Superlattices, Phys. Rev. Lett. **124**, 187601 (2020).

[57] J. Liu and X. Dai, Theories for the correlated insulating states and quantum anomalous Hall effect phenomena in twisted bilayer graphene, Phys. Rev. B **103**, 035427 (2021).

[58] S. Liu, E. Khalaf, J. Y. Lee, and A. Vishwanath, Nematic topological semimetal and insulator in magic-angle bilayer graphene at charge neutrality, Phys. Rev. Res. **3**, 013033 (2021).

[59] B. Lian, Z.-D. Song, N. Regnault, D. K. Efetov, A. Yazdani, and B. A. Bernevig, Twisted bilayer graphene. IV. Exact insulator ground states and phase diagram, Phys. Rev. B **103**, 205414 (2021).

[60] B.-B. Chen, Y. D. Liao, Z. Chen, O. Vafek, J. Kang, W. Li, and Z. Y. Meng, Realization of topological Mott insulator in a twisted bilayer graphene lattice model, Nat. Commun. **12**, 5480 (2021).

[61] Y. Xie, A. T. Pierce, J. M. Park, D. E. Parker, E. Khalaf, P. Ledwith, Y. Cao, S. H. Lee, S. Chen, P. R. Forrester, K. Watanabe, T. Taniguchi, A. Vishwanath, P. Jarillo-Herrero, and A. Yacoby, Fractional Chern insulators in magic-angle twisted bilayer graphene, Nature (London) **600**, 439 (2021).

[62] G. Shavit, E. Berg, A. Stern, and Y. Oreg, Theory of Correlated Insulators and Superconductivity in Twisted Bilayer Graphene, Phys. Rev. Lett. **127**, 247703 (2021).

[63] J. Kang, B. A. Bernevig, and O. Vafek, Cascades between Light and Heavy Fermions in the Normal State of Magic-Angle Twisted Bilayer Graphene, Phys. Rev. Lett. **127**, 266402 (2021).

[64] P. Potasz, M. Xie, and A. H. MacDonald, Exact Diagonalization for Magic-Angle Twisted Bilayer Graphene, Phys. Rev. Lett. **127**, 147203 (2021).

[65] Y. Da Liao, J. Kang, C. N. Breiø, X. Y. Xu, H.-Q. Wu, B. M. Andersen, R. M. Fernandes, and Z. Y. Meng, Correlation-Induced Insulating Topological Phases at Charge Neutrality in Twisted Bilayer Graphene, Phys. Rev. X **11**, 011014 (2021).

[66] L. Klebl, Z. A. H. Goodwin, A. A. Mostofi, D. M. Kennes, and J. Lischner, Importance of long-ranged electron-electron interactions for the magnetic phase diagram of twisted bilayer graphene, Phys. Rev. B **103**, 195127 (2021).

[67] Y. H. Kwan, G. Wagner, T. Soejima, M. P. Zaletel, S. H. Simon, S. A. Parameswaran, and N. Bultinck, Kekulé Spiral Order at All Nonzero Integer Fillings in Twisted Bilayer Graphene, Phys. Rev. X **11**, 041063 (2021).

[68] D. V. Chichinadze, L. Classen, Y. Wang, and A. V. Chubukov, SU(4) Symmetry in Twisted Bilayer Graphene: An Itinerant Perspective, Phys. Rev. Lett. **128**, 227601 (2022).

[69] G. Wagner, Y. H. Kwan, N. Bultinck, S. H. Simon, and S. A. Parameswaran, Global Phase Diagram of the Normal State of Twisted Bilayer Graphene, Phys. Rev. Lett. **128**, 156401 (2022).

[70] Z.-D. Song and B. A. Bernevig, Magic-Angle Twisted Bilayer Graphene as a Topological Heavy Fermion Problem, Phys. Rev. Lett. **129**, 047601 (2022).

[71] H. C. Po, H. Watanabe, and A. Vishwanath, Fragile Topology and Wannier Obstructions, Phys. Rev. Lett. **121**, 126402 (2018).

[72] H. C. Po, L. Zou, T. Senthil, and A. Vishwanath, Faithful tight-binding models and fragile topology of magic-angle bilayer graphene, Phys. Rev. B **99**, 195455 (2019).

[73] J. Kang and O. Vafek, Symmetry, Maximally Localized Wannier States, and a Low-Energy Model for Twisted Bilayer Graphene Narrow Bands, Phys. Rev. X **8**, 031088 (2018).

[74] M. Koshino, N. F. Q. Yuan, T. Koretsune, M. Ochi, K. Kuroki, and L. Fu, Maximally Localized Wannier Orbitals and the Extended Hubbard Model for Twisted Bilayer Graphene, Phys. Rev. X **8**, 031087 (2018).

[75] N. F. Q. Yuan and L. Fu, Model for the metal-insulator transition in graphene superlattices and beyond, Phys. Rev. B **98**, 045103 (2018).

[76] F. D. M. Haldane, Model for a Quantum Hall Effect without Landau Levels: Condensed-Matter Realization of the "Parity Anomaly," Phys. Rev. Lett. **61**, 2015 (1988).